Lattice-BGK simulation of a two-dimensional channel flow around a square cylinder

Vol 12 No 1, January 2003
1009-1963/2003/12(01)/0067-08

Chinese Physics

Lattice-BGK simulation of a two-dimensional channel flow around a square cylinder*

Guo Wei-Bin(郭卫斌)[a], Wang Neng-Chao(王能超)[a,b],
Shi Bao-Chang(施保昌)[b,†], and Guo Zhao-Li(郭照立)[c]

[a] *School of Computer Science and Technology, Huazhong University of Science and Technology, Wuhan 430074, China*
[b] *Parallel Computing Institute, Huazhong University of Science and Technology, Wuhan 430074, China*
[c] *State Key Laboratory of Coal Combustion, Huazhong University of Science and Technology, Wuhan 430074, China*

(Received 21 June 2002; revised manuscript received 28 July 2002)

The confined flow around a square cylinder mounted inside a two-dimensional channel (blockage ratio $\beta = 1/8$) was investigated in detail by a newly developed incompressible nonuniform lattice-BGK model. It is found that the vortex shedding behind the cylinder induces periodicity in the flow field, and the periodicity of the flow will lose for $Re > 300$. A detailed analysis for a range of Reynolds numbers between 1 and 500 was presented. Quantitative comparisons with other methods show that the model gives accurate results for complex flows.

Keywords: lattice-BGK method, square cylinder, Strouhal number, drag coefficient
PACC: 4760, 4710, 0550

1. Introduction

In recent years the lattice-Boltzmann method (LBM) has attracted much attention in the simulation of a wide range of complex fluid flow problems. Typical examples are steady plane Poiseuille flow,[1] thermal viscous cavity flow,[2] multiphase flows and high-speed compressible flows,[3,4], etc. The success of this method can be partly attributed to the particle-based approach which is directly inherited from its predecessor, the lattice gas automata (LGA). Unlike LGA, the LBM simulates a flow system by tracking the evolution of particle distributions instead of tracking single particles. For this reason, it overcomes some of the inherent limitations of the LGA, such as statistical noise, non-Galilean invariance. Compared with other traditional computational fluid dynamics methods, such as the finite difference schemes, the major advantage of LBM is that it provides a good insight into the underlying microscopic dynamics of the physical system investigated, whereas most methods focus only on the solution of the macroscopic equations.[5,6]

The flow around bluff bodies in a two-dimensional (2D) channel has been an attraction in all kinds of fluid mechanical investigations for a long time. This flow situation is popular not only because of its academic attractiveness but also owing to its related technical problems associated with the energy conservation and the structural design of buildings, bridges, towers, cars, masts and wires, etc.[7–11] Much work has been done in simulating 2D flow around such bluff obstacles in the past. In particular, the 2D flow around circular cylinders has been studied extensively. In contrast to many theoretical, experimental, and numerical data on the flow around circular cylinders over a wide range of Reynolds numbers, there are very few similar studies and information on the flow around square bodies.[8,11] Previous investigations of the flow around circular cylinders performed with the LBM clearly show that this method is an appropriate tool for such kinds of flows.[12]

In this work we investigate the vortex-shedding phenomena and the topology of the vortex structure behind the square cylinder in a 2D duct, which changes with Reynolds numbers, so as to understand the dynamical behaviour of the flow. Again, the influence of the Reynolds number on the lift and drag forces is also the aim of this paper. Simulation results in a range of Reynolds numbers between 1 and 500 are

*Project supported by the National Natural Science Foundation of China (Grant No 60073044), and the State Key Development Programme for Basic Research of China (Grant No G1999022207).
†Author to whom correspondence should be addressed. E-mail: sbchust@wuhan.cngb.com

presented, and are thoroughly compared with other numerical data with respect to the Strouhal number, lift and drag coefficients.

2.Specification of the problem

The system of interest is a horizontal channel with an obstacle in the form of a square cylinder positioned inside it. The problem domain and specified boundary conditions are shown in Fig.1. The inflow is located X_{u} units upstream of the cylinder. The outflow is located X_{d} units downstream of the cylinder. The size of the obstacle, D, and the channel height, H, define the solid blockage of the confined flow (blockage ratio $\beta = D/H$).

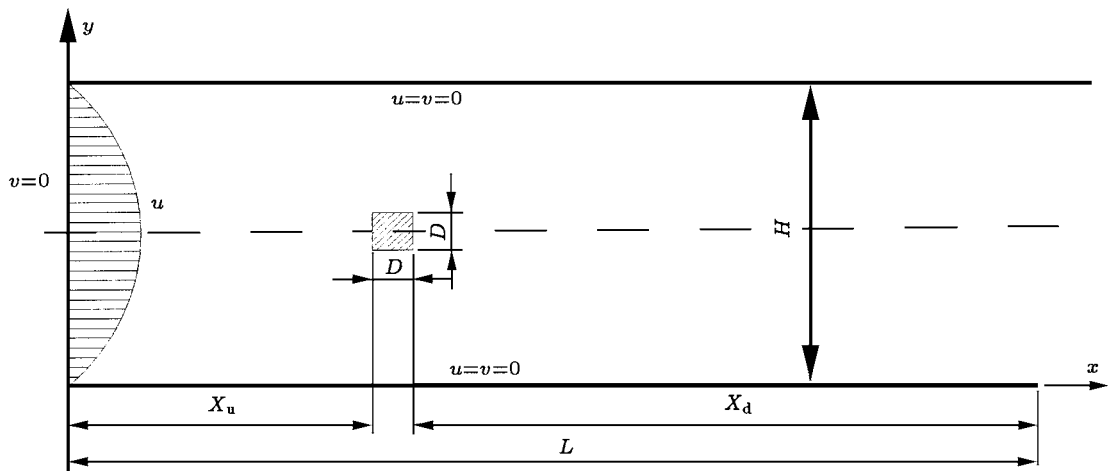

Fig.1. Computational domain and boundary conditions.

The dimensionless equations for continuity and momentum may be expressed as

$$\nabla \cdot \boldsymbol{u} = 0, \tag{1}$$

$$\frac{\partial \boldsymbol{u}}{\partial t} + \nabla \cdot (\boldsymbol{u}\boldsymbol{u}) = -\nabla p + Re^{-1}\nabla^2 \boldsymbol{u}, \tag{2}$$

where $Re = u_{\max} D/v$ is the Reynolds number. Here $u_{\max}$ is the maximum flow velocity of the parabolic inflow profile and v is the kinematic viscosity.

The boundary conditions in this investigation are as follows. At the inlet, a parabolic velocity inflow profile is applied. The outflow boundary condition for velocity is $\partial u/\partial x = \partial v/\partial x = 0$. No-slip boundary conditions are prescribed at the body surfaces. At the top and bottom surfaces of the channel, symmetry conditions simulating a frictionless wall are used ($u = v = 0$). The normal derivative for the pressure is set to zero at all boundaries. The normal derivative in the diagonal direction for the pressure is also set to zero at all corners of the flow field.

3. Numerical method

For the computations, a 2D 9-bit incompressible lattice-Boltzmann model (id2q9) with single time Bhatnagar–Gross–Krook (BGK) relaxation collision operator $\Omega_i(t) = -\frac{1}{\tau}(g_i - g_i^{(0)})$ proposed by Guo *et al*[12] is used

$$\begin{aligned} &g_i(\boldsymbol{x} + c\boldsymbol{e}_i\Delta t, t + \Delta t) - g_i(\boldsymbol{x}, t) \\ &= -\frac{1}{\tau}[g_i(\boldsymbol{x}, t) - g_i^{(0)}(\boldsymbol{x}, t)], \end{aligned} \tag{3}$$

where subscript i indicates the velocity direction (i runs from 0 to 8), and Δx and Δt are the lattice grid spacing and the time step, respectively. The particle speed, c, is defined as $c = \Delta x/\Delta t$. The dimensionless relaxation time τ is related to the kinematic viscosity as $v = \frac{(2\tau - 1)}{6}\frac{(\Delta x)^2}{\Delta t}$. And $g_i(\boldsymbol{x}, t)$ is the density distribution function associated with the particle at node $\boldsymbol{x}$ and time t with velocity $\boldsymbol{e}_i$; $g_i^{(0)}(\boldsymbol{x}, t)$ is the corresponding local equilibrium distribution function, which is determined by

$$g_i^{(0)} = \alpha_i p + s_i(\boldsymbol{u}), \tag{4}$$

where $\alpha_0 = -4\sigma/c^2$, $\alpha_i = \lambda/c^2$ for i=1,2,3,4, and $\alpha_i = \gamma/c^2$ for i=5,6,7,8. Parameters σ, λ, and γ satisfy $\lambda + \gamma = \sigma$, $\lambda + 2\gamma = 1/2$. $s_i(\boldsymbol{u})$ is given by

$$s_i(\boldsymbol{u}) = \omega_i\left[3\frac{(\boldsymbol{e}_i \cdot \boldsymbol{u})}{c} + 4.5\frac{(\boldsymbol{e}_i \cdot \boldsymbol{u})^2}{c^2} - 1.5\frac{|\boldsymbol{u}|^2}{c^2}\right], \tag{5}$$

with the weight factors $\omega_0 = 4/9$, $\omega_i = 1/9$ for i=1,2,3,4, and $\omega_i = 1/36$ for i=5,6,7,8. The macroscopic velocity and pressure of the flow are calculated

from the distribution function

$$\boldsymbol{u} = \sum_{i=1}^{8} c\boldsymbol{e}_i g_i, \quad p = \frac{c^2}{4\sigma}\left[\sum_{i=1}^{8} g_i + s_0(\boldsymbol{u})\right]. \qquad (6)$$

Although this scheme has proved to be very promising, it has some potential shortcomings compared with the traditional state-of-the-art numerical methods, like the finite-element method. The uniformity of the lattice is one of them. From a computational point of view nonuniform grids can be efficient for computing fluid flows because the grid resolution can be adapted to the spatial complexity of the flow dynamics. Thus, in this work we use a newly developed approach (DDLBM),[13] allowing lattice-BGK simulations on nonuniform grids. The basic idea of DDLBM is to decompose the whole flow field into some relatively regular subdomains, and then perform simulations on each subdomain using id2q9 model with uniform grid. The interpolation between interfaces is carried out in order to couple the subdomains consistently. The DDLBM solves a flow problem by general lattice-BGK model in each subdomain and does not need to establish new model. Another distinctive feature is that the interpolation procedure is done only at boundaries of subdomains, which can significantly reduce the computational time.

4. Results and discussions

The flow pattern with a Reynolds number range $1 \leq Re \leq 500$ has been investigated numerically on a 80×500 lattice. For the Reynolds numbers considered in this paper, it is known from experiments and other numerical studies that vortex shedding is observed and a 2D time-dependent flow evolves. At a Reynolds number Re above approximately 300, the flow might become three-dimensional (3D), and 2D computations will therefore produce unphysical results.[9] In simulations, all the results were normalized to allow comparisons between this paper and other results, i.e. velocities were normalized with $u_{\max}$, physical times with $D/u_{\max}$, and frequencies with $u_{\max}/D$. Force and pressure coefficients were normalized with the dynamic pressure, $\rho u_{\max}^2/2$. For all cases considered, the channel length L and width H were set to 500 and 80, respectively, and the obstacle of a size 10×10 in lattice unit was positioned at $L/3$ downstream the entrance of the channel. The blockage ratio was fixed at β=0.125. The relaxation parameter $w = 1/\tau$ for Re=1, 30, 62, 133, 300, 500 was set to be 0.3, 0.95, 1.2, 1.55, 1.8, and 1.91, respectively. The computational region Ω was divided into two subdomains Ω_1 and Ω_2 (see Fig.2). Here, Ω_1 was a square domain whose left-side and right-side virtual boundaries were BL=156 and BR=196, respectively. The lower and upper boundaries were BD=20 and BU=60, respectively. The subdomain Ω_2 was $\Omega_2 = \Omega - \Omega_1$. The lattice size for Ω_1 was 160×160. The id2q9 model was used on Ω_1 and Ω_2. Hence, the refinement factor was $n = \Delta x_2/\Delta x_1 = 4$. In this paper, for boundary conditions, the nonequilibrium extrapolation method proposed by Guo *et al*[14] is used.

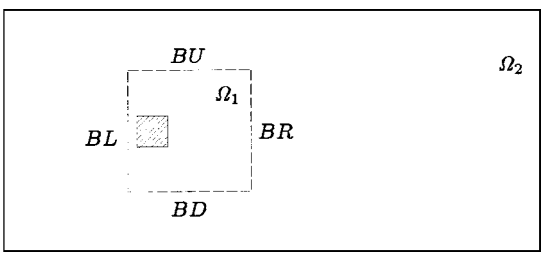

Fig.2. Domain decomposition.

The flow with Re=1 was first simulated. The pressure was initialized to be p=0, and the velocities at all nodes, except for the nodes at the inflow boundary, were set to $u = v = 0$. The streamline contours are shown in Fig.3. Figure 4 shows the vorticity contours corresponding to the streamline patterns presented in Fig.3. As shown in Figs.3(a) and 4(a), for $Re \leq 1$, the creeping steady flow passes the square cylinder, and no separation takes place. As Re increases, the flow separates first at the trailing edge of the cylinder and a closed steady recirculation region is observed. The length of the recirculation region increases linearly with Re. The flow pattern is perfectly symmetric with respect to the oncoming flow and the vortex shedding has not started. Whereas for $Re > Re_c$, where Re_c is between Re=60 and 62, the symmetry eventually breaks down. With increasing Reynolds number, after a sufficient number of iterations, the flow becomes periodic and evolves with a fixed frequency f. At Re=80, the separation point of the vortices is observed to be the rear edge of the obstacle and moves from the rear to the front edge of the obstacle with higher Reynolds numbers. When Re is further increased, a von Karman vortex street is formed and alternate shedding of vortices into the stream becomes prominent. At Re=133, small secondary vortices can be found at the top and bottom of the obstacle and the separation is observed at the

leading edge of the square cylinder. The flow field in front of the cylinder for Re=80–300 is nearly independent of the structure of the wake. Within this range of Reynolds numbers, the above plots also show clearly the effect of the Reynolds number on the flow pattern, and the flow can still be considered to be 2D.

For $Re > 300$, no steady solution is found (see Fig.4(f)). The result for $Re > 300$ oscillates between a series of different configurations. Flow at these Reynolds numbers eventually becomes 3D and turbulent.[9,10] For this reason, the results presented in this paper are those for Re up to 500. All the flow structures in our simulation compare well with the previous flow visualization and numerical simulations.

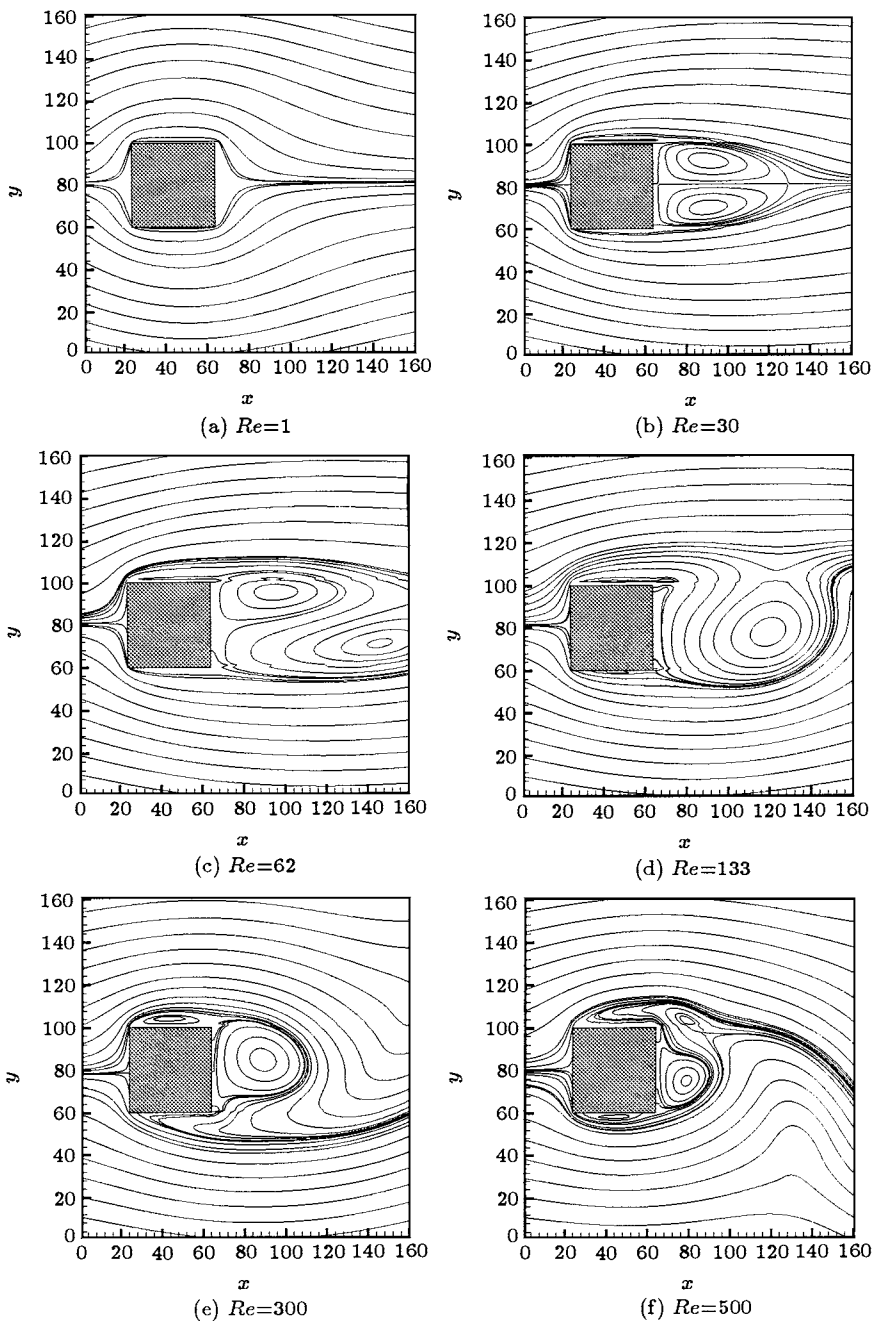

Fig.3. Streamlines around the square cylinder for different Reynolds numbers.

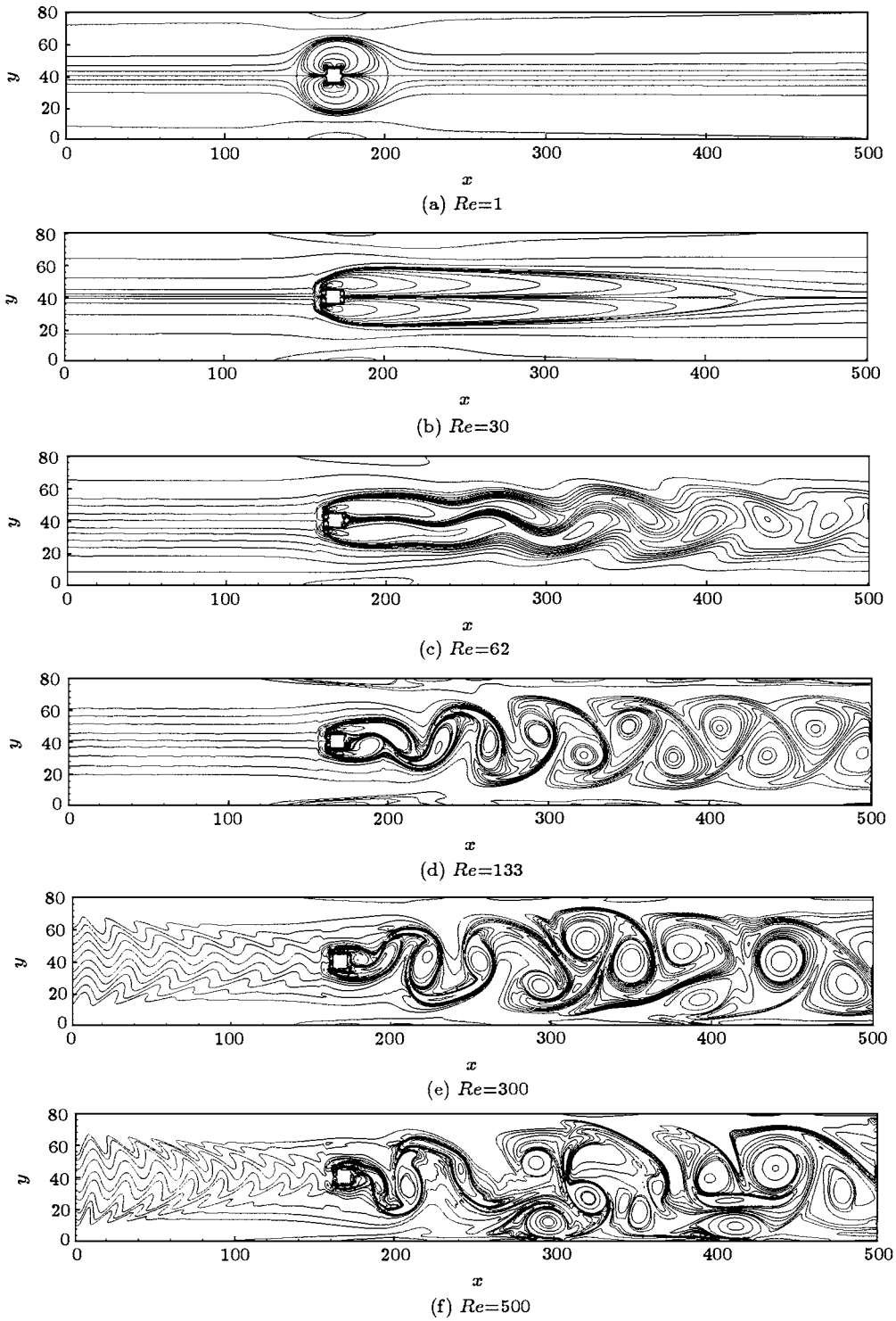

(a) Re=1

(b) Re=30

(c) Re=62

(d) Re=133

(e) Re=300

(f) Re=500

Fig.4. Vorticity contours around the square cylinder for different Reynolds numbers.

To quantify the results, the Strouhal number St is plotted as a function of the Reynolds number Re in Fig.5. Here, the Strouhal number is defined as

$$St = \frac{f_s \cdot D}{u_{max}}, \tag{7}$$

where f_s is the vortex shedding frequency which is determined by spectral analysis of the temporal evolution of the v-component or u-component of the flow velocity at several points in the wake behind the obstacle. It can also be measured from the time evolution plot of the lift or drag coefficient distribution, namely C_l or C_d. Figure 6 depicts the time evolution of the monitored velocity component (v) and the lift coefficient at Re=100. As seen from Fig.5, the present method yields a somewhat lower Strouhal number in the entire range of Reynolds number compared with, but the present Strouhal number distribution fits quite well with that in Refs.[8], [11] and [15]. Our method, furthermore, shows that the Strouhal number has no dependence on the grid resolution.

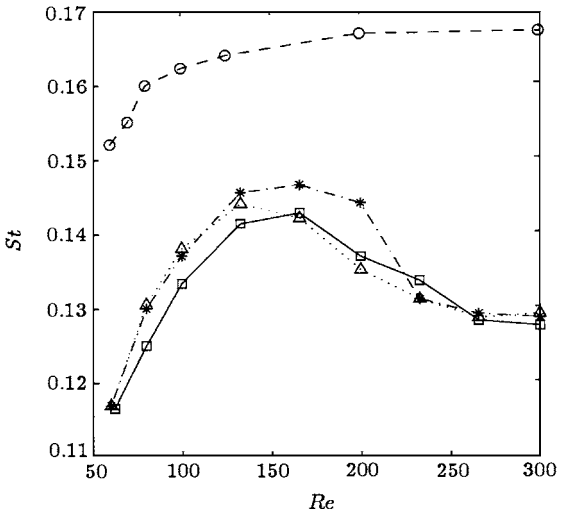

Fig.5. Strouhal numbers St for different Reynolds numbers. △: Bernsdorf (LBA:2000×320), –∗–: Bernsdorf (FVM: 500×80), –○–: Mukhopadhyay, –□– : present work.

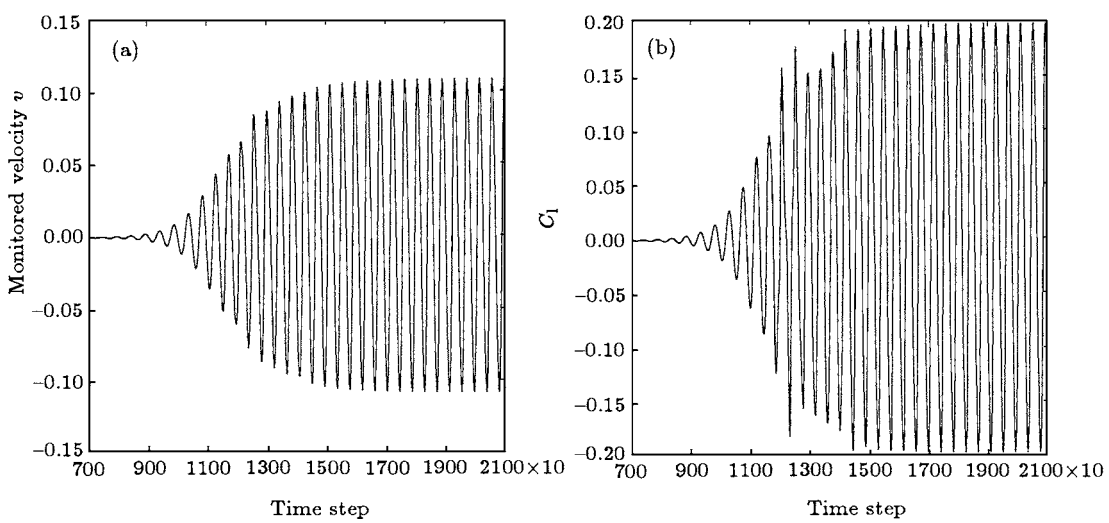

Fig.6. Signal traces of velocity component (v) in the wake and time evolution of lift coefficient: (a) signal traces of velocity component (v) in the wake; (b) time evolution of lift coefficient.

Other important quantities taken into account in this paper are the drag and lift coefficients. The drag coefficient, C_d, and the lift coefficient, C_l, are calculated using

$$C_d = \frac{1}{\frac{1}{2}\rho u_{max}^2 D} F_x, \qquad C_l = \frac{1}{\frac{1}{2}\rho u_{max}^2 D} F_y,$$

where F_x and F_y are, respectively, the drag force and lift force on the cylinder. Figures 7 and 8 show the drag coefficient C_d, the variation of the drag coefficient ($\max(C_d)$-$\min(C_d)$) and the lift coefficient ($\max(C_l)$-$\min(C_l)$) in the Re range $1 \leq Re \leq 500$, respectively. As shown in the figures, this paper provides reliable and accurate results.

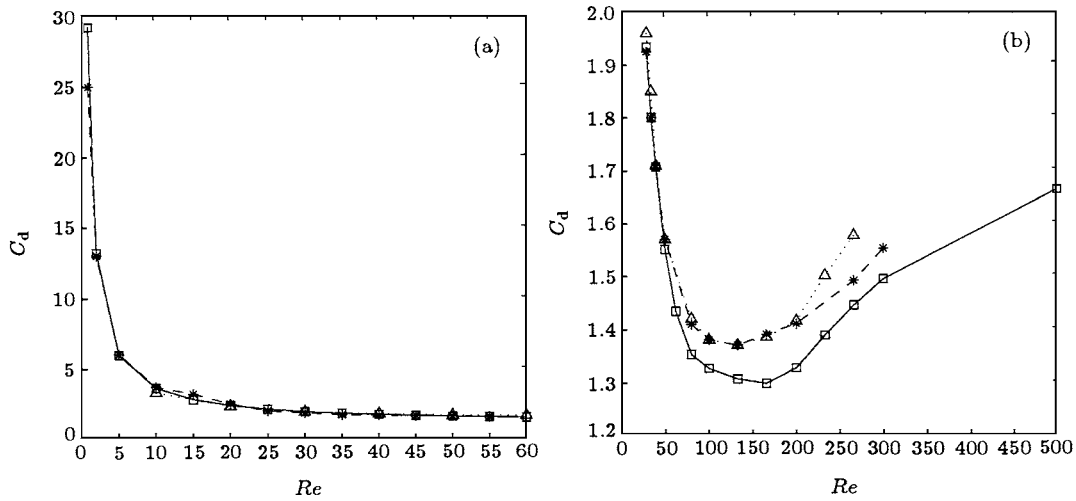

Fig.7. Computed time-averaged drag coefficient C_d versus Reynolds number Re: (a) steady flow; (b) unsteady flow. △: Bernsdorf (LBA) (EQ:2000×320), –∗–: Bernsdorf (FVM) (EQ: 500×80), –□–: present work.

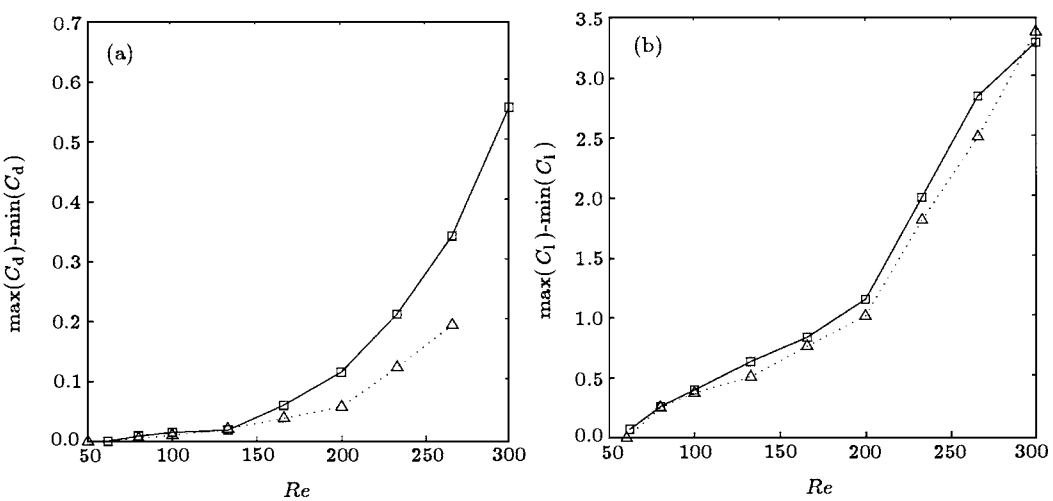

Fig.8. Variation of force coefficient versus Reynolds number Re: (a) drag variation, max(C_d)-min(C_d); (b) lift variation, max(C_l)-min(C_l). △: Bernsdorf (FVM) (EQ:500×80), –□–: present work.

5. Conclusions

A lack of accurate and detailed data was found in the literature for the confined channel flow past around a cylinder, thus initiated this paper. In order to generate reliable numerical results, a newly developed incompressible nonuniform lattice-BGK model was applied to investigate the 2D flow around a square cylinder inside a channel ($\beta = 0.125$) in the Reynolds number range $1 \leq Re \leq 500$. Strouhal numbers, drag and lift coefficients were computed and compared with the scattered data in the literature. We have shown that our implementation of the lattice-BGK approach yields reliable results. By employing the id2q9 model, the compressible effect is eliminated efficiently. Compared with the uniform lattice-BGK model, nonuniform lattice-BGK model significantly reduces the computational time and can be used to find some local details in the flow fields. We will further use these methods to simulate 3D channel flow around a square cylinder in the future.

During simulation, since the maximum velocity and the lattice size are limited, the relaxation parameter, w, needs to be large to achieve the higher Reynolds numbers. It is found that the lowest value of w leading to stable simulations depends on the Mach number. The appropriate value of c is about 6.5–12.

On the other hand, to obtain a reliable simulation, w should not be too close to its upper limit. It must be less than 2 to ensure positive viscosity.

It is apparent that further building up of both suitable equilibrium distribution function and new boundary conditions is needed. Applying the lattice-BGK method to other complex flows is a challenging work.

Acknowledgements

We would like to thank Professor B L Zhang, Y X Li, and L S Kang for helpful discussions concerning the lattice Boltzmann method and domain decomposition technique.

References

[1] Chopard B and Masselot A 1999 *Future Gen. Comput. Syst.* **16** 249
[2] Lü X Y and Li H B 2001 *Acta Phys. Sin.* **50** 422 (in Chinese)
[3] Fang H P *et al* 2000 *Chin. Phys.* **9** 515
[4] Feng S D and Michihisa T 2001 *Acta Phys. Sin.* **50** 1006 (in Chinese)
[5] Shi B C *et al* 2001 *Proc. DCABES* (Wuhan: Hubei Science and Technology Press) p107
[6] Shi B C *et al* 2002 *Chin. Phys. Lett.* **19** 515
[7] He X Y and Doolen G 1997 *J. Comput. Phys.* **134** 306
[8] Bernsdorf J *et al* 1998 *Int. J. Mod. Phys.* C **9** 1129
[9] Sohankar A *et al* 1998 *Int. J. Num. Meth. Fluids* **26** 39
[10] Wissink J G 1997 *Int. J. Num. Meth. Fluids* **25** 51
[11] Mukhopadhyay A *et al* 1992 *Int. J. Num. Meth. Fluids* **14** 1473
[12] Guo Z L *et al* 2000 *J. Comput. Phys.* **165** 288
[13] Guo Z L *et al* 2001 *Chin. J. Comput. Phys.* **18** 181 (in Chinese)
[14] Guo Z L *et al* 2002 *Chin. Phys.* **11** 366
[15] Breuer M *et al* 2000 *Int. J. Heat Fluid Flow* **21** 186